This is an open access article published under an ACS AuthorChoice License, which permits copying and redistribution of the article or any adaptations for non-commercial purposes.

CHEMISTRY OF MATERIALS
Cite This: Chem. Mater. 2018, 30, 5593−5601
Article
pubs.acs.org/cm

Liquid Phase Acoustic Wave Exfoliation of Layered MoS_2: Critical Impact of Electric Field in Efficiency

Md Mohiuddin,[†] Yichao Wang,[‡] Ali Zavabeti,[†] Nitu Syed,[†] Robi S. Datta,[†] Heba Ahmed,[§] Torben Daeneke,[†] Salvy P. Russo,[∥] Amgad R. Rezk,[§] Leslie Y. Yeo,*[,§] and Kourosh Kalantar-Zadeh*[,⊥,†]

[†]School of Engineering, [§]Micro/Nanophysics Research Laboratory, School of Engineering, and [∥]ARC Centre of Excellence in Exciton Science, School of Science, RMIT University, Melbourne, Victoria 3000, Australia

[‡]School of Life and Environmental Sciences, Deakin University, Melbourne, Victoria 3216, Australia

[⊥]School of Chemical Engineering, University of New South Wales, Sydney, New South Wales 2052, Australia

Supporting Information

ABSTRACT: Liquid phase exfoliation techniques of layered crystals establish the basis for high yield production of two-dimensional (2D) flakes suspension. However, such techniques generally require a long processing time. The recent demonstration of the piezoelectric phenomenon in noncentrosymmetric layered transition metal dichalcogenides, such as molybdenum disulfide (MoS_2), leads to new opportunities for fast and efficient exfoliation processes. Here we use concomitant electric field and mechanical shear force for producing a suspension of MoS_2 nanoflakes from exfoliation of their layered bulk powder particles. The electrical and mechanical fields are applied by a surface acoustic wave (SAW) microcentrifugation device. We show that the overall yield per unit of time of 3.816%/h can be achieved, which is at least an order of magnitude larger than previously reported liquid phase exfoliation methods. Simultaneously, the impressive monolayer yield is 58% in an excellent agreement with the computational estimation based on electric field assisted density functional theory calculations. The work therefore reports two major advancements. We show efficient exfoliation of layered MoS_2. More importantly, we demonstrate the importance of the electric field in increasing the efficiency of liquid phase exfoliation. It is thus expected that these outcomes to fundamentally impact research activities focused on the exfoliation of piezoelectric 2D materials.

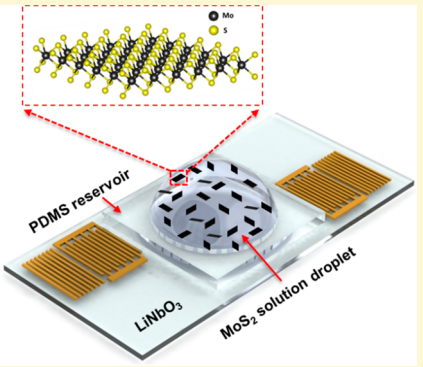

INTRODUCTION

Liquid phase exfoliation is a common method for obtaining high yield suspensions of two-dimensional (2D) transition metal dichalcogenide flakes.[1−3] Different liquid phase exfoliation methods including mechanical blending and grinding, and also shear mixing (or a combination of them) have been developed.[2−8] These techniques may require a long processing time and sometimes a low proportion of monolayers are achieved.[7−10] A high population of monolayers can be exfoliated by liquid phase ion intercalation processes; however, such methods are still time-consuming, require hazardous solvents, and contribute to phase transformation.[3,11−15]

A pathway to increase the efficiency of exfoliating noncentrosymmetric layered crystals is to devise a process based on surface acoustic waves (SAWs). A SAW is a nanometer-order amplitude mechanical wave, accompanying an electric field, which propagates along the surface of a piezoelectric substrate. The extremely large surface acceleration along the substrate as the SAW traverses is an efficient means for driving liquid actuation at the microscale,[16−18] including microcentrifugation flows that will be exploited in this work to exfoliate the flakes.

The concomitant electric field with the mechanical wave in that constitutes the SAW[19,20] can be advantageous for enhancing the exfoliation process of layered transition metal dichalcogenides, such as 2H MoS_2 under specific conditions. Adjacent planes of 2H MoS_2 are held together by weak van der Waals forces to form the bulk of the crystal. The stacking arrangement of adjacent atomic layers in bulk 2H MoS_2 makes it centrosymmetric, which does not show piezoelectricity. In contrast, dimensionally reduced monolayered or odd layered MoS_2 exhibits strong piezoelectricity due to their noncentrosymmetric crystal structure.[21,22] The piezoelectricity depends on the number of layers. For example, the piezoelectric coupling coefficient of monolayer MoS_2 is 3 times higher than that of trilayer.[22] Such noncentrosymmetric behavior, hence emergence of piezoelectricity, is also observed for the outer planes on each side the 2H MoS_2 bulk.

Given the piezoelectricity of noncentrosymmetric 2H MoS_2, the SAW induced electric field exerts a force on the top

Received: April 12, 2018
Revised: July 19, 2018
Published: July 20, 2018

Downloaded via RMIT UNIV on May 18, 2021 at 00:06:43 (UTC).
See https://pubs.acs.org/sharingguidelines for options on how to legitimately share published articles.

© 2018 American Chemical Society

DOI: 10.1021/acs.chemmater.8b01506
Chem. Mater. 2018, 30, 5593−5601

piezoelectric layer of the bulk 2H MoS_2 or the flakes that are made of an odd number of layers. This is in addition to the mechanical shear imparted on the material, regardless of whether it is centrosymmetric or noncentrosymmetric, by the SAW and the flow it induces in the liquid. It is expected that the combination of the shear force and electric field make the exfoliation process much more efficient. On the basis of this assumption, we therefore utilize a microcentrifugation process to exfoliate layered 2H MoS_2. In particular, we demonstrate that the thickness of layered MoS_2 can be tuned through controlled manipulation of the SAW exposure duration, and verify the experimental results for the number of layers we obtained with a computational prediction.

EXPERIMENTAL SECTION

Fabrication of the SAW Device. Optically surface polished 500 μm thick single crystal 128° Y-rotated lithium niobate (128° YX $LiNbO_3$) wafer was used as the substrate on which two sets of interdigital transducers (IDTs, Figure S1, Supporting Information) were patterned using a standard UV photolithography process.[23] Each IDT comprised 20 finger pairs. Additionally, a reflector is patterned in parallel to each IDT to reflect the acoustic waves from the devices' edges back to the position where the liquid is deposited on the SAW device. These reflectors each comprise 20 metal strips with each finger has possessing a width of 50 μm. As such, in IDTs, each metallic finger pairs and their associated spacing, has a width of 200 μm, resulting in a similar wavelength that excites the resonance frequency of ~19.2 MHz (see Figure S2, Supporting Information) for SAW traveling at 3850 m s^{-1}. A setup consisting of a RF signal generator (N10149, Agilent) and power amplifier (ZHL-5W-1) were used to drive the IDTs at the resonance frequency using an applied sinusoidal electric field.

Preparation of PDMS Reservoir. Prepolymer of polydimethylsiloxane (PDMS) and curing agent (Dow Corning Corporation, USA) were mixed with a weight ratio of 10:1, and the mixture was poured into a plastic Petri dish to form a ~1.5 mm height. This was then degassed in a vacuum desiccator and cured in a vacuum oven at 80 °C. After the curing process, the PDMS reservoir was prepared by punching a 4 mm diameter hole. For sealing of the PDMS reservoir onto the SAW substrate, oxygen plasma was used for 30 s at 400 mTorr in a pressurized chamber (Harrick Plasma, Max Power 200W). The PDMS reservoir was subsequently pressed against the substrate immediately after the surfaces treatment and then heated in an oven at 80 °C for 1 h.

Sample Preparation and Characterization. A sample of 20 mg of MoS_2 powder (99.9% purity, 0.8−1.2 μm size, US Research Nanomaterials, Inc.) was added to 10 mL of Milli-Q water (bulk MoS_2 powder; Figure S3, Supporting Information). Tween 20 (0.05 mg mL^{-1}, VWR) was then added into the mix to stabilize the dispersion. After exfoliation with the SAW, the MoS_2 nanoflakes in the supernatant were collected for further characterization after centrifugation for 30 min at 2000 rpm. Transmission electron microscopy (TEM) images were acquired using JEOL1010 whereas high resolution TEM (HRTEM) imaging was performed in both JEOL2010 and JEOL2100F. Samples for TEM imaging were prepared by drop-casting the water suspended 2D MoS_2 flakes onto TEM grids. Nanoflake thickness measurements were performed with Bruker Dimension Icon atomic force microscopy (AFM) in ScanAsyst (air) mode. Exfoliated MoS_2 was drop casted onto gold coated silicon substrates and Raman analysis of the samples were performed under ambient conditions using a Jobin Yvon Horiba TRIAX 320 spectrometer fitted with a 100× magnification lens (60 s with 3 accumulations, 532 nm excitation wavelengths). X-ray photoelectron spectroscopy (XPS) measurements were performed using Thermo K-Alpha at pass energy of 100 eV for the peak scans. The instrument uses an Al Kα monochromated X-ray source (1486.7 eV), with a spot size of approximately 400 μm.

Computational Methods. The Gaussian basis set *ab initio* package CRYSTAL14 was used in hybrid spin dependent density functional theory (DFT) calculations.[24,25] The B3LYP hybrid exchange−correlation functional was employed augmented with an empirical London-type correction to the energy to include dispersion contributions to the total energy.[26] The correction term is based on the Grimme method, which has been used with B3LYP for calculating cohesive energies in dispersion bonded molecular crystals.[27,28] For sulfur, the Durand effective core pseudopotential (ECP) was used to account for the core electrons in sulfur and 1 31G* basis sets for the valence electrons. For molybdenum, a Hay−Wadt small-core ECP was used in order to account for the 28 core electrons and a 311-31G basis set for the valence electrons.[29] Periodically infinite, 1−9 layer MoS_2 nanoflakes were constructed from a geometry optimized MoS_2 bulk structure, and their nanoflake energies, under an applied electric field (perpendicular to the surface of the nanoflake), were calculated using DFT (B3LYP) and the method described by Grimme to calculate the dispersion forces. 15 × 15 × 1 *k*-point sampling was used for converging the electronic ground state.[27,28] This method has been successfully previously applied to MoS_2 and SnS_2 nanoflakes calculations.[30,31]

RESULTS AND DISCUSSION

Standard lithography was employed to pattern the SAW device, construct the PDMS reservoir, and seal it onto the transducer, as presented in the Experimental Section. Figure 1A shows a schematic diagram of the microcentrifugation SAW

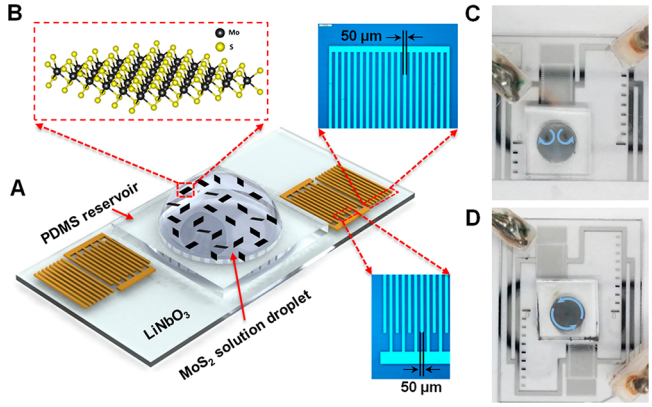

Figure 1. Illustration and photographs of microcentrifugation SAW devices. (A) Illustration of an asymmetric microcentrifugation SAW device constituting the lithium niobate chip with a PDMS reservoir bonded onto it. The insets show the IDTs, reflectors, and their dimensions. (B) Illustration of monolayer MoS_2 structure. (C) Centered droplet aligned with a single IDT on the device giving rise to two stable acoustic streaming vortices in the droplet. (D) Azimuthal acoustic streaming circulation in the droplet as a consequence of the asymmetric positioning of the droplet confined in the reservoir, which is placed off-center with respect to the two opposing IDTs. The video of D can be found in Movie S1 (Supporting Information).

device that incorporates a PDMS reservoir for the exfoliation of MoS_2. A droplet (17 μL) of 2H MoS_2 nanoparticles (2 mg mL^{-1}) placed into the PDMS reservoir and the SAW device is excited at ~3 W (14 V) and ~19.2 MHz. Illustration of a monolayer MoS_2 after the exfoliation process represented in Figure 1B.

When a high frequency propagating SAW encounters the liquid droplet in its path, as shown in Figure 1A, it leaks its energy into the liquid. This produces a compressional wave in the liquid, which, as a consequence of viscous attenuation in

DOI: 10.1021/acs.chemmater.8b01506
Chem. Mater. 2018, 30, 5593−5601

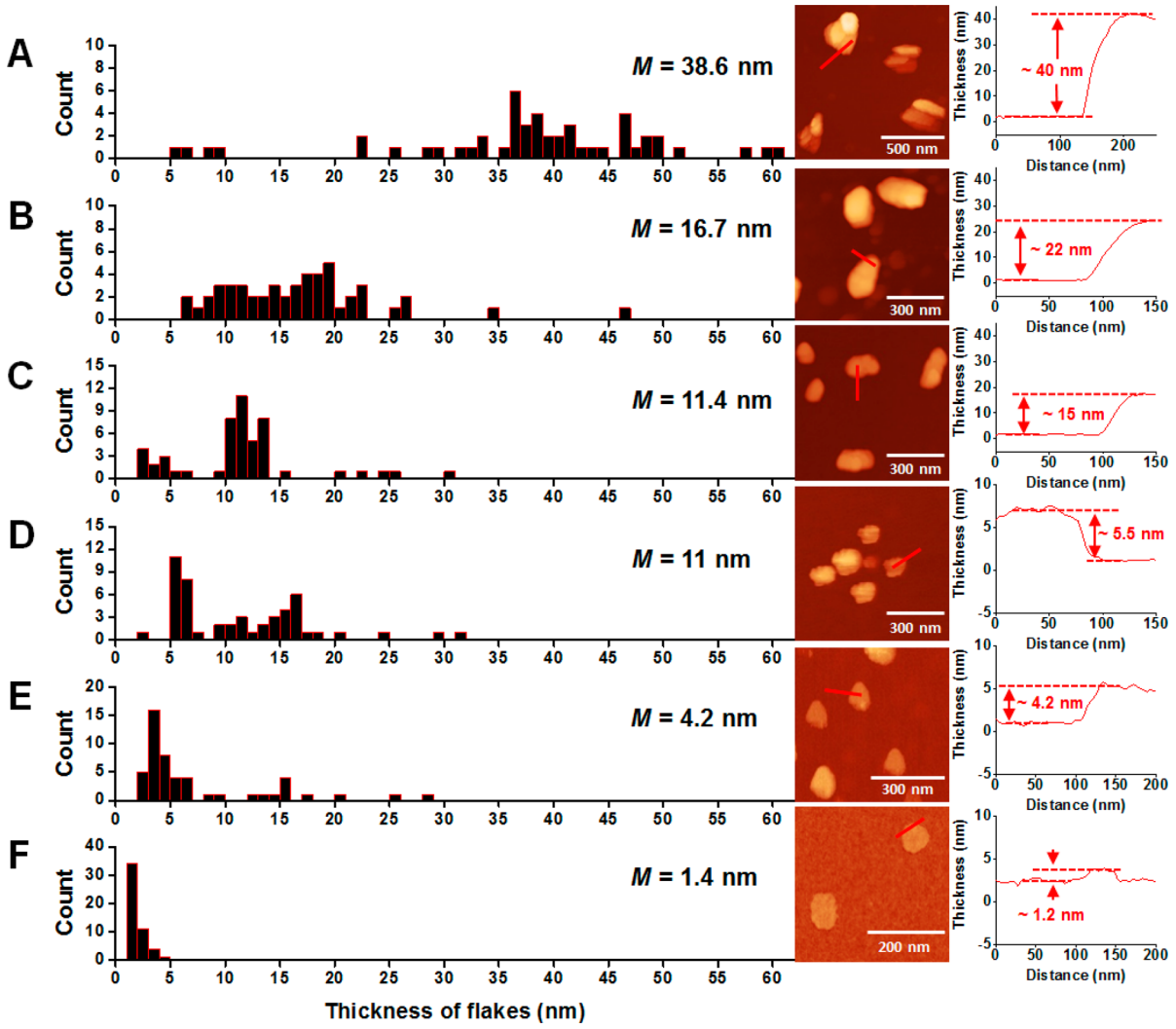

Figure 2. Characterization of thickness distribution. Thickness distribution histograms of the exfoliated MoS_2 nanoflakes, obtained from the AFM measurements, along with typical images and height profile at different SAW exposure durations of (A) 1, (B) 5, (C) 10, (D) 15, (E) 20, and (F) 25 min. It can be seen that the SAW exfoliation process requires at least 25 min to produce monolayers of MoS_2 nanoflakes effectively. *M* represents the median thickness in the resolution of 0.1 nm.

the liquid media, induces strong acoustic streaming within the droplet (as depicted by the blue arrows in Figure 1C,D).[17] We note that the in-plane component of the SAW beneath the liquid droplet suffers from minimal attenuation since the droplet actuation is mainly driven by the out-of-plane component.[32] The degree of symmetry associated with the droplet streaming is a function of the waves propagation direction, the droplet position and the boundaries of the reservoir.[18,33] A symmetric streaming pattern comprising two quasi-steady vortices can be seen if the liquid droplet is positioned in the center of acoustic wave propagation path (Figure 1C), whereas an asymmetric pattern leading to azimuthal streaming is generated if the liquid droplet is placed off-center with respect to the SAW radiation (Figure 1D). We found the latter configuration to be more effective for exfoliation, due to the large streaming velocities ~0.15 m s^{-1} that can be attained. As discussed previously in Li et al., dispersion of the MoS_2 particles occurs under the intense streaming above a threshold velocity, RF (radio frequency) power, MoS_2 flake properties, and liquid surface tension are the dominant factors directly correlating the effective thickness-modulation of MoS_2.[33] Powers lower than 0.3 W were insufficient to produce any streaming flows, and beyond 3 W liquid atomization was observed. As such, 3 W RF power was consistently used throughout the experimental study. Low concentration surfactant was used (see Experimental Section) in our experiments to stabilize the exfoliated flake dispersions. The importance of this method is that the process can be scaled-up by using parallel arrays of devices. Parallel arrays of low cost microcentrifugation SAW devices (~USD $1/device) can be integrated for potential large-scale throughput as well long-term device operation. The modules of those chips can be operated simultaneously. The idea of such scaling up has been demonstrated in a versatile modular plug-and-actuate concept of microarray titer plate[34] that can be adopted for the mass production of MoS_2. The scaling up of our proof-of-concept work presented in this article utilizing the intrinsic piezoelectric properties of MoS_2 using SAW devices, will be demonstrated in a future article. In order to investigate and obtain a better insight into the performance of the system, the exfoliated MoS_2 nanoflakes at different SAW exposure durations were experimentally characterized with AFM, TEM, and Raman spectroscopy.

DOI: 10.1021/acs.chemmater.8b01506
Chem. Mater. 2018, 30, 5593−5601

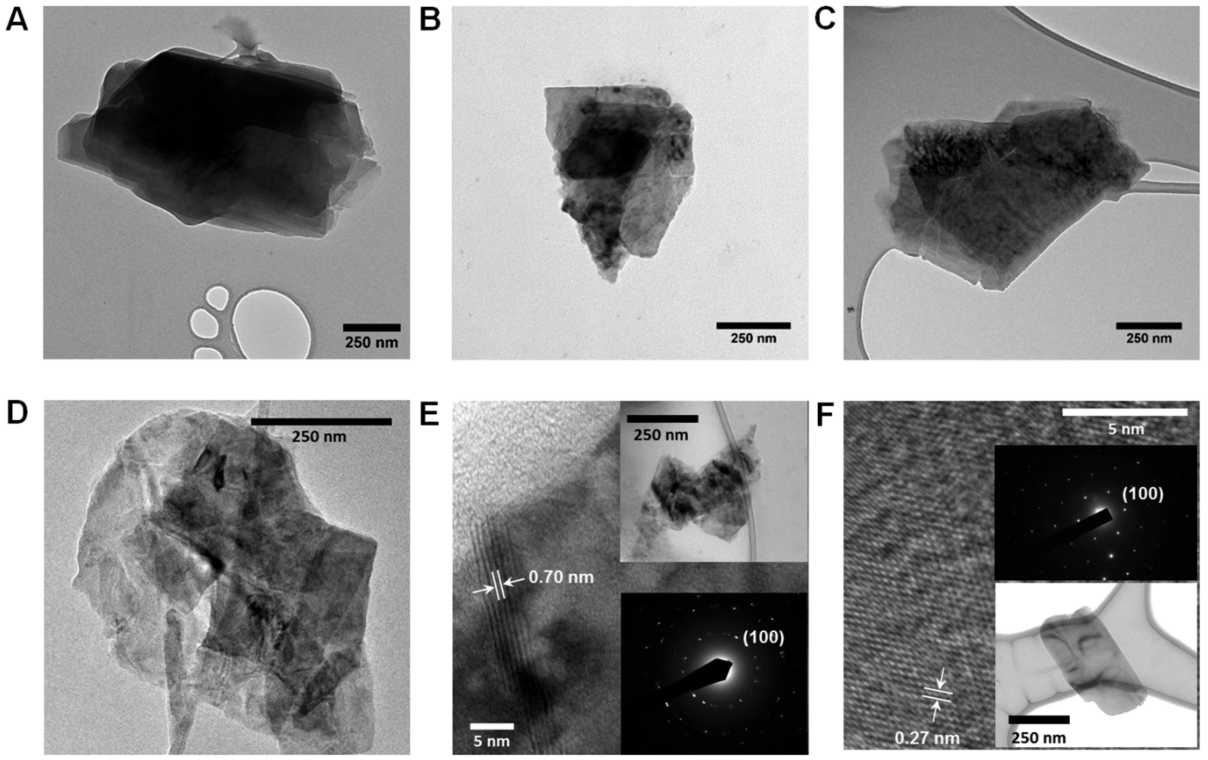

Figure 3. Microscopic characterization of exfoliated nanoflakes. TEM images of the MoS_2 nanoflakes exfoliated from bulk 2H MoS_2 for different SAW exposure durations: (A) 1 min, (B) 5 min, (C) 10 min, and (D) 15 min. (E) HRTEM of the 20 min sample with corresponding SAED and TEM image represented in the inset. (F) HRTEM of the 25 min sample with TEM and SAED (inset).

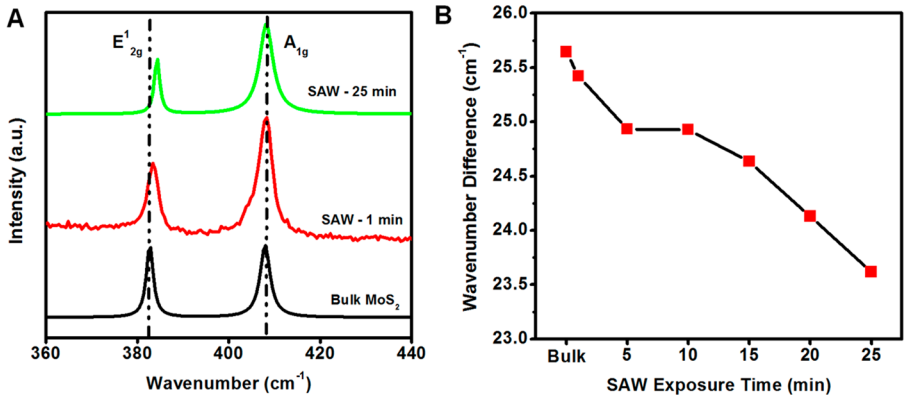

Figure 4. Structure characterization of exfoliated nanoflakes. (A) Raman spectra of the exfoliated MoS_2 nanoflakes at different exfoliation durations. (B) Wavenumber difference of the E^1_{2g} and A_{1g} Raman modes as a function of SAW exposure time.

Approximately 10 μL of the supernatant solutions was drop-casted onto Si substrates and imaged by AFM to estimate the surface topography and thickness profile of the nanoflakes. Figure 2 represents the AFM images with thickness distribution histograms for the exfoliated nanoflakes obtained from 1 to 25 min SAW exposed samples.

A total of 50 nanoflakes were used for the construction of the histograms for all cases. The flakes showed a large thickness distribution for the 1 min SAW exposed sample with a majority in the range 36−42 nm (median of 38.6 nm). The median for the thickness distribution of nanoflakes continued to shift to lower values with increasing exposure time (Figure 2). The SAW exfoliation process became monolayer dominant at 25 min exposure. After this exposure duration, the majority of the nanoflakes' thicknesses ranged between ∼1.2 and ∼2 nm corresponding to monolayer and double layer of MoS_2 with the presence of surfactant residual.[35,36] The frequency of monolayers obtained is relatively high (58%) for the 25 min case in comparison to other liquid exfoliation methods, and an analysis of performance is presented later in this text. Moreover, the 25 min sample exhibits a constricted width normal distribution curve in comparison to more expanded distributions for other exfoliation durations. It is important to consider that the forces applied to the particles consist of electric field and also shear forces. These shear forces exist during the exfoliation and are generated by the SAW acoustic streaming. Even numbered flakes that are not affected by electric field are exfoliated due to this shear force generated inside the droplet by the SAW streaming; therefore, a thick even number of layers is absent in the 25 min SAW exfoliated sample. The exfoliation trend is clearly seen in Figure 2, and the median thickness of the flakes constantly decreases from 1

DOI: 10.1021/acs.chemmater.8b01506
Chem. Mater. 2018, 30, 5593−5601

to 25 min due to both SAW streaming and the electric field. However, the monolayers, which are predicted on the basis of the mathematical simulations (presented later in this text), are mostly seen at 25 min time, and that is the duration that the electric field effect dominates the process.

To further investigate the exfoliation process, TEM of all samples were obtained and representative examples are shown in Figure 3 along with the HRTEM and selected area electron diffraction (SAED) of the long run samples (20 and 25 min). The TEM images are in general agreement with AFM topographies. Highly crystalline, defect free MoS_2 nanoflakes are observed in HRTEM images. HRTEM and the SAED show the hexagonal lattice structure of single crystalline MoS_2 with a fringe spacing of ∼0.27 nm corresponding to the (100) lattice planes.[30] The layer spacing in samples with several in-registry planes is 0.7 nm.

Micro-Raman spectroscopy was conducted to assess the vibrational modes of MoS_2 nanoflakes obtained with the different SAW exposure durations. The E^1_{2g} and A_{1g} modes are considered as they are the thickness dependent modes. As the MoS_2 crystal is dimensionally reduced, the in-plane (E^1_{2g}) mode of the bulk crystal, whose peak occurs at ∼382 cm^{-1}, stiffens (thus blue-shifted) and, conversely, the out-of-plane (A_{1g}) mode, whose peak occurs at ∼407 cm^{-1}, softens (hence red-shifted).[37] The wavenumber difference between the two main Raman peaks (E^1_{2g} and A_{1g}) is shown in Figure 4A for bulk, 1, and 25 min SAW exfoliated samples. The 25 min SAW exfoliated sample possesses the smallest wavenumber difference (23.62 cm^{-1}) in comparison with that of the bulk (25.64 cm^{-1}).[38,39] The full wavenumber versus exfoliation time curve is presented in Figure 4B. In accordance with AFM, the wavenumber difference decreases with increasing SAW exposure duration and hence the reduction in the number of layers. The difference of wavenumbers in vibrational peaks (E^1_{2g} and A_{1g}) never reaches those smaller values compared to the previous reports that are representative of monolayers.[37] Such a discrepancy is likely due to the effect of residues on flakes and also polydispersity of nanoflake thicknesses, which have been similarly reported previously.[39−41]

The binding energies of the samples were studied using XPS. The results for the bulk powder and 25 min SAW exfoliated samples are presented in Figure S4 (Supporting Information). Both samples show doublet Mo $3d_{5/2}$ and Mo $3d_{3/2}$ peaks at 229.4 and 232.6 eV, respectively. The binding energies of the S doublet were also seen at 162.2 and 163.1 eV, representing S $2p_{3/2}$ and $2p_{1/2}$, respectively. This means that the exfoliated materials comprised stoichiometric MoS_2 and that the exfoliation process did not deteriorate the quality of the flakes.

Thermogravimetric analysis (TGA) was utilized for the yield estimation[42] described in the Supporting Information (Figure S5). The concentration of the exfoliated MoS_2 nanoflakes was measured as ∼32 $\mu g\ mL^{-1}$, which translates into ∼3.816%/h yield per unit of time obtained at 1000 rpm centrifugation.

Figure 5A presents an illustration of MoS_2 centrosymmetric even layers and noncentrosymmetric odd layers. Figure 5B shows the relative proportion of the number of fundamental layers in the 2D MoS_2 flakes after 25 min of SAW exfoliation. Extracted from the results in Figure 2F, approximately 58% of the produced flakes are monolayers, as presented in Figure 5B. On the basis of our our calculations, this exfoliation takes place under an applied electric field of on average 10^5 V m^{-1} generated by the SAW device. This electric field was estimated from the applied voltage (14 V) across the IDTs, the width of the IDT finger pairs, and the possible penetration depth of the wave into the aqueous media.[20]

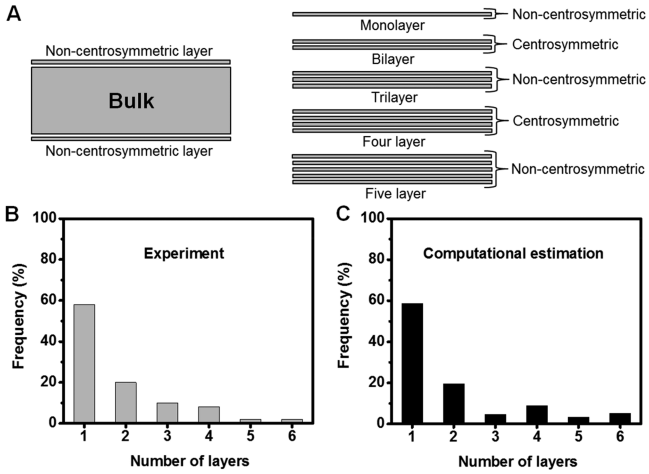

Figure 5. Computational estimation and validation of exfoliation. (A) Illustration of centrosymmetric and noncentrosymmetric MoS_2 layers. (B) Number of layers in the 25 min SAW exposed sample obtained from the AFM thickness distribution estimation compared with (C) exfoliation of nine-layer nanoflakes under the influence of an electric field in the computational estimation.

To understand the mechanism that underpins the SAW exfoliation process, we conducted a computational assessment. In our model, we assume that the exfoliation is mediated by the electric displacement under an applied electric field. This would only occur if a structure is noncentrosymmetric (i.e., it has no inversion symmetry). Group theory reveals that flakes of MoS_2 with an odd number of layers are noncentrosymmetric and thereby exhibit piezoelectricity, while sheets with even number of layers of MoS_2 have fundamental planes that are centrosymmetric and are therefore not piezoelectric.[22] Therefore, a further assumption in our model is that once an even numbered layer has been created, no further exfoliation of that nanoflake can occur. Additionally, electric fields induced displacement between MoS_2 fundamental planes is only possible when the thicknesses of odd layer of nanoflakes are reasonably low (<7 layers) to exhibit appreciable piezoelectricity.[22]

As a simplifying assumption, the numbers of layers in the bulk can be considered for computation. Here the example for 9 layers is shown that can be extended to smaller numbers (highly likely as piezoelectricity increases) or larger numbers (less likely as the thickness is closer to bulk and piezoelectricity drops) using the same method. As can be seen in the Figure S6, exfoliation events can be continued through to a maximum of 4 exfoliation steps (labeled as "branch layers" in Figure S6, Supporting Information). Here we only account for the possibility of single and double exfoliation events. In this example, starting from a 9-layer nanoflake the exfoliation possibilities include 8−1, 7−2, 6−3, 5−4 as single exfoliation events and 7−1−1, 5−3−1, 3−3−3 as double exfoliation events. We can label a single exfoliation event as ($k|k-n$, n), which means a k-layer MoS_2 slab has exfoliated into a $k-n$ layer slab and an n-layer slab. Similarly, double exfoliation events are labeled as ($k|k-n_1-n_2$, n_1, n_2).

Mathematically, an exfoliation proportional probability weighting (P) is associated with each of the events using in an n layer system as

DOI: 10.1021/acs.chemmater.8b01506
Chem. Mater. 2018, 30, 5593−5601

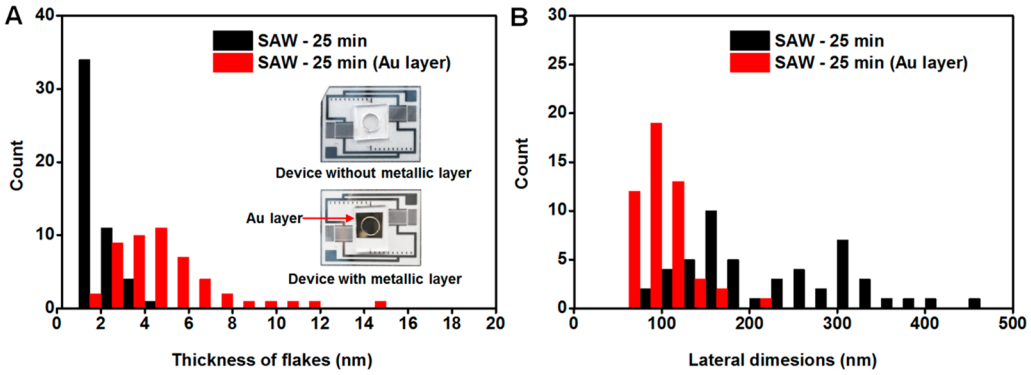

Figure 6. Comparison of shear force only exfoliation with electric field assisted exfoliation. (A) AFM thickness distribution histograms of MoS_2 flakes (25 min) with (black) and without (red) the presence of the electric field. Inset shows microcentrifugation SAW device coated with Au layer underneath the PDMS reservoir and device without any metallic layer. (B) Flakes lateral dimension histograms.

$$p \propto e^{-|\Delta E|/kT} \quad (1)$$

where k is the Boltzmann's constant and T is the temperature and ΔE is the difference of exfoliation energy before and after the exfoliation event as calculated using a hybrid DFT computation (B3LYP). Under the 9-layer assumption, possible pathways for single and double exfoliation events are represented in Figure S6 (Supporting Information). Exfoliation events continue when the outcome contains odd number of layers. They stop when exfoliation results in either even layer or monolayer flakes. A description of how we calculated the frequency of the exfoliated MoS_2 layers, with the number of layers, is presented in the Supporting Information.

The computational outcomes are presented in Figure 5C, which is in good agreement with the measurements. For instance, the ratio of monolayer MoS_2 in experiment and computation estimations are ~58% and ~59%, respectively. The slight discrepancies between the experiment and computation estimation of other flake numbers may originate from the fact that shear exfoliation, which was not considered in the computational estimation, still plays an important role in the exfoliation process.

The shear rate is crucial for the exfoliation of the monolayer using probe sonication or turbulent based techniques.[6,43,44] In reports based on such techniques, efficient exfoliation to ultrathin layers generally occurs when the shear rate exceeds the threshold value of $\sim 10^4$ s^{-1}.[6,43,44] Considering the streaming velocity of the microcentrifugation SAW device and the diameter of the PDMS reservoir, the shear rate produced in our microcentrifugation SAW device is $\sim 10^2$ s^{-1}, which is relatively low.

To investigate the exfoliation characteristics of MoS_2 nanoflakes using a microcentrifugation SAW device in the absence of the electric field, a thin 100 nm gold (Au) layer (with 30 nm chromium adhesion layer) deposited between the PDMS reservoir and lithium niobate substrate (Figure 6A inset). This metallic layer screens and prevents electric field exposure to MoS_2 particles. The flake thickness distribution histogram shown in Figure 6A represents the exfoliation of MoS_2 (25 min) with and without the presence of the electric field. As can be seen, shear force exfoliation (in red), with no electric field, has a larger median value for the flakes thickness (4.3 nm) in comparison with the presence of the electric field (1.4 nm). This red bar distribution is very similar to previous experiments using the shear force only, confirming that electric field is not present.[7] Obviously the experiment also shows the increased efficiency of the exfoliation process in the presence of the electric field. Figure 6B shows the corresponding lateral dimension histograms of flakes of Figure 6A. As can be seen, the average lateral dimension of the exfoliated samples in the presence of the electric field is larger than that of only shear force exfoliation. It seems that the electric field helps in the more efficient exfoliation of the crystal before they are broken down by the shear force. Therefore, both experiment and computational analysis suggest that the electric field plays a dominant role in exfoliating MoS_2 to ultrathin layers.

We have compared the efficiency of our technique with a few selected previous works in terms of the median number of layers, the run time, and the yield per unit of time (Table 1).

Table 1. Comparison of the Exfoliation Efficiency of MoS_2 Prepared in This Work with That Produced from Selected Other Comparable Single Step Liquid Exfoliation Methods

exfoliation methods, chemical used	median number of layers	run time	yield per unit of time, %/h	ref
Liquid exfoliation using SAW with aqueous surfactant	1	25 min	3.816	this work
Liquid exfoliation using blender with aqueous surfactant	2−12	2 h	0.400	7
Probe sonication with aqueous surfactant	4	16 h	0.625	45
Probe sonication with NMP	-	7 h	0.285	46
Probe sonication with NMP	-	140 h	0.290	5

To facilitate consistency in the comparison, the data in the table only focus on liquid exfoliation techniques with surfactants or chemical solvents, without the incorporation of any assisting chemically active reagents (such as butyllithium and sodium hydroxide). As can be seen, the proposed method here has the best exfoliation efficiency in an impressively short time, resulting in approximately 58% monolayer MoS_2 flakes. In our work, the yield is high, reaching a yield per unit of time of 3.816%/h. This is higher than that of previous reports for sonication methods with surfactant or *N*-methyl-2-pyrrolidone (NMP) as a solvent. Such efficiency can be ascribed to our ability to exploit the piezoelectricity of the noncetrosymmetric material, given the presence of the electric field that

DOI: 10.1021/acs.chemmater.8b01506
Chem. Mater. 2018, 30, 5593−5601

accompanies the mechanical shear, which is not possible with other methods.

CONCLUSIONS

In brief, unlike conventional exfoliation methods, a compact microcentrifugation SAW device was developed that applies a concomitant electric field and mechanical shear force for efficient exfoliation of a monolayer enriched MoS_2 suspension. Overall, a yield per unit of time of 3.816%/h was achieved utilizing the developed SAW system, which is at least 5 times higher than the best previously reported value. High accelerating acoustic wave induced shear streaming reduces the thickness of MoS_2. Through the experimental realization and computational estimation, it was shown that the electric field plays a critical role in increasing the efficiency of the exfoliation process due to the intrinsic piezoelectric nature of noncentrocymmetric layered MoS_2. The thickness of MoS_2 can be modulated by increasing the SAW exfoliation duration, as revealed by the AFM images that show the existence of a high percentage of MoS_2 monolayers. Further optimization studies on the design and development of the device is expected to improve the production efficiency.

The SAW system reveals the possibility of microscale routes for the versatile exfoliation of noncentrosymmetric layered materials and also alludes to the significant possibility of exploiting the electric field to increase the efficiency of these exfoliation processes. The process can be applied to a large number of layered crystals including transition metal oxides and chalcogenides. A list of possible candidates is presented in the works by Duerloo et al. and Blonsky et al.[21,47] Additionally, many more layered crystals should be explored and identified on the basis of the selection criteria of noncentrosymmetric condition.

ASSOCIATED CONTENT

Supporting Information

The Supporting Information is available free of charge on the ACS Publications website at DOI: 10.1021/acs.chemmater.8b01506.

SAW device configuration; reflection coefficient (S_{11}) of SAW device; SEM of bulk MoS_2; XPS of both bulk and exfoliated MoS_2; TGA of exfoliated MoS_2; calculation of theoretical prediction of frequency of exfoliated MoS_2 layers with the number of layers (PDF)

Exfoliation of MoS_2 nanoflakes using microcentrifugation SAW device (MPG)

AUTHOR INFORMATION

Corresponding Authors

*L. Y. Yeo. E-mail: leslie.yeo@rmit.edu.au.

*K. Kalantar-Zadeh. E-mail: k.kalantar-zadeh@unsw.edu.au, kourosh.kalantar@rmit.edu.au.

ORCID

Torben Daeneke: 0000-0003-1142-8646

Leslie Y. Yeo: 0000-0002-5949-9729

Kourosh Kalantar-Zadeh: 0000-0001-6109-132X

Author Contributions

K.K., M.M., and A.R.R. conceived the original research idea and supervised the project. M.M. carried out the device development, sample synthesis, and characterizations. A.Z., N.S., R.S.D., and H.A. carried out parts of the characterizations. Y.W. performed the HRTEM imaging. S.P.R. designed, developed, and interpreted the DFT simulations. M.M. wrote the manuscript with the help of A.R.R., L.Y.Y., and K.K. All the authors contributed, discussed, and commented on the manuscript.

Notes

The authors declare no competing financial interest.

ACKNOWLEDGMENTS

We thank the assistance of the RMIT Microscopy and Microanalysis Facility (RMMF) and the RMIT Micro Nano Research Facility (MNRF). A.R.R. is grateful for RMIT Vice-Chancellor's Research Fellowship. L.Y.Y. is a recipient of a Future Fellowship from the Australian Research Council under grant FT130100672. K.K. and T.D. acknowledge funding received from the ARC Centre of Excellence in Future Low-Energy Electronics Technologies (FLEET) (CE170100039).

REFERENCES

(1) Nicolosi, V.; Chhowalla, M.; Kanatzidis, M. G.; Strano, M. S.; Coleman, J. N. Liquid exfoliation of layered materials. *Science* **2013**, *340*, 1226419.

(2) Chen, Y.; Tan, C.; Zhang, H.; Wang, L. Two-dimensional graphene analogues for biomedical applications. *Chem. Soc. Rev.* **2015**, *44*, 2681−2701.

(3) Ferrari, A. C.; Bonaccorso, F.; Fal'ko, V.; Novoselov, K. S.; Roche, S.; Boggild, P.; Borini, S.; Koppens, F. H. L.; Palermo, V.; Pugno, N.; Garrido, J. A.; Sordan, R.; Bianco, A.; Ballerini, L.; Prato, M.; Lidorikis, E.; Kivioja, J.; Marinelli, C.; Ryhanen, T.; Morpurgo, A.; Coleman, J. N.; Nicolosi, V.; Colombo, L.; Fert, A.; Garcia-Hernandez, M.; Bachtold, A.; Schneider, G. F.; Guinea, F.; Dekker, C.; Barbone, M.; Sun, Z.; Galiotis, C.; Grigorenko, A. N.; Konstantatos, G.; Kis, A.; Katsnelson, M.; Vandersypen, L.; Loiseau, A.; Morandi, V.; Neumaier, D.; Treossi, E.; Pellegrini, V.; Polini, M.; Tredicucci, A.; Williams, G. M.; Hee Hong, B.; Ahn, J.-H.; Min Kim, J.; Zirath, H.; van Wees, B. J.; van der Zant, H.; Occhipinti, L.; Di Matteo, A.; Kinloch, I. A.; Seyller, T.; Quesnel, E.; Feng, X.; Teo, K.; Rupesinghe, N.; Hakonen, P.; Neil, S. R. T.; Tannock, Q.; Lofwander, T.; Kinaret, J. Science and technology roadmap for graphene, related two-dimensional crystals, and hybrid systems. *Nanoscale* **2015**, *7*, 4598−4810.

(4) Novoselov, K. S.; Jiang, D.; Schedin, F.; Booth, T. J.; Khotkevich, V. V.; Morozov, S. V.; Geim, A. K. Two-dimensional atomic crystals. *Proc. Natl. Acad. Sci. U. S. A.* **2005**, *102*, 10451−10453.

(5) O'Neill, A.; Khan, U.; Coleman, J. N. Preparation of high concentration dispersions of exfoliated MoS_2 with increased flake size. *Chem. Mater.* **2012**, *24*, 2414−2421.

(6) Paton, K. R.; Varrla, E.; Backes, C.; Smith, R. J.; Khan, U.; O'Neill, A.; Boland, C.; Lotya, M.; Istrate, O. M.; King, P.; Higgins, T.; Barwich, S.; May, P.; Puczkarski, P.; Ahmed, I.; Moebius, M.; Pettersson, H.; Long, E.; Coelho, J.; O'Brien, S. E.; McGuire, E. K.; Sanchez, B. M.; Duesberg, G. S.; McEvoy, N.; Pennycook, T. J.; Downing, C.; Crossley, A.; Nicolosi, V.; Coleman, J. N. Scalable production of large quantities of defect-free few-layer graphene by shear exfoliation in liquids. *Nat. Mater.* **2014**, *13*, 624−630.

(7) Varrla, E.; Backes, C.; Paton, K. R.; Harvey, A.; Gholamvand, Z.; McCauley, J.; Coleman, J. N. Large-scale production of size-controlled MoS_2 nanosheets by shear exfoliation. *Chem. Mater.* **2015**, *27*, 1129−1139.

(8) Yao, Y.; Lin, Z.; Li, Z.; Song, X.; Moon, K.-S.; Wong, C.-p. Large-scale production of two-dimensional nanosheets. *J. Mater. Chem.* **2012**, *22*, 13494−13499.

(9) Kim, J.; Kwon, S.; Cho, D.-H.; Kang, B.; Kwon, H.; Kim, Y.; Park, S. O.; Jung, G. Y.; Shin, E.; Kim, W.-G.; Lee, H.; Ryu, G. H.; Choi, M.; Kim, T. H.; Oh, J.; Park, S.; Kwak, S. K.; Yoon, S. W.; Byun, D.; Lee, Z.; Lee, C. Direct exfoliation and dispersion of two-

DOI: 10.1021/acs.chemmater.8b01506
Chem. Mater. 2018, 30, 5593−5601

dimensional materials in pure water *via* temperature control. *Nat. Commun.* **2015**, *6*, 8294.
(10) Yao, Y.; Tolentino, L.; Yang, Z.; Song, X.; Zhang, W.; Chen, Y.; Wong, C. p. High-concentration aqueous dispersions of MoS_2. *Adv. Funct. Mater.* **2013**, *23*, 3577−3583.
(11) Fan, X.; Xu, P.; Li, Y. C.; Zhou, D.; Sun, Y.; Nguyen, M. A. T.; Terrones, M.; Mallouk, T. E. Controlled exfoliation of MoS_2 crystals into trilayer nanosheets. *J. Am. Chem. Soc.* **2016**, *138*, 5143−5149.
(12) Fan, X.; Xu, P.; Zhou, D.; Sun, Y.; Li, Y. C.; Nguyen, M. A. T.; Terrones, M.; Mallouk, T. E. Fast and efficient preparation of exfoliated 2H MoS_2 nanosheets by sonication-assisted lithium intercalation and infrared laser-induced 1T to 2H phase reversion. *Nano Lett.* **2015**, *15*, 5956−5960.
(13) Ramakrishna Matte, H. S. S.; Gomathi, A.; Manna, A. K.; Late, D. J.; Datta, R.; Pati, S. K.; Rao, C. N. R. MoS_2 and WS_2 analogues of graphene. *Angew. Chem., Int. Ed.* **2010**, *49*, 4059−4062.
(14) Wang, Y.; Carey, B. J.; Zhang, W.; Chrimes, A. F.; Chen, L.; Kalantar-Zadeh, K.; Ou, J. Z.; Daeneke, T. Intercalated 2D MoS_2 utilizing a simulated sun assisted process: reducing the HER overpotential. *J. Phys. Chem. C* **2016**, *120*, 2447−2455.
(15) Wang, Q. H.; Kalantar-Zadeh, K.; Kis, A.; Coleman, J. N.; Strano, M. S. Electronics and optoelectronics of two-dimensional transition metal dichalcogenides. *Nat. Nanotechnol.* **2012**, *7*, 699−712.
(16) Destgeer, G.; Jung, J. H.; Park, J.; Ahmed, H.; Sung, H. J. Particle separation inside a sessile droplet with variable contact angle using surface acoustic waves. *Anal. Chem.* **2017**, *89*, 736−744.
(17) Yeo, L. Y.; Friend, J. R. Surface acoustic wave microfluidics. *Annu. Rev. Fluid Mech.* **2014**, *46*, 379−406.
(18) Shilton, R.; Tan, M. K.; Yeo, L. Y.; Friend, J. R. Particle concentration and mixing in microdrops driven by focused surface acoustic waves. *J. Appl. Phys.* **2008**, *104*, 014910.
(19) Rezk, A. R.; Carey, B.; Chrimes, A. F.; Lau, D. W. M.; Gibson, B. C.; Zheng, C.; Fuhrer, M. S.; Yeo, L. Y.; Kalantar-Zadeh, K. Acoustically-driven trion and exciton modulation in piezoelectric two-dimensional MoS_2. *Nano Lett.* **2016**, *16*, 849−855.
(20) Miansari, M.; Qi, A.; Yeo, L. Y.; Friend, J. R. Vibration-induced deagglomeration and shear-induced alignment of carbon nanotubes in air. *Adv. Funct. Mater.* **2015**, *25*, 1014−1023.
(21) Duerloo, K.-A. N.; Ong, M. T.; Reed, E. J. Intrinsic piezoelectricity in two-dimensional materials. *J. Phys. Chem. Lett.* **2012**, *3*, 2871−2876.
(22) Wu, W.; Wang, L.; Li, Y.; Zhang, F.; Lin, L.; Niu, S.; Chenet, D.; Zhang, X.; Hao, Y.; Heinz, T. F.; Hone, J.; Wang, Z. L. Piezoelectricity of single-atomic-layer MoS_2 for energy conversion and piezotronics. *Nature* **2014**, *514*, 470−474.
(23) Gracioso Martins, A. M.; Glass, N. R.; Harrison, S.; Rezk, A. R.; Porter, N. A.; Carpenter, P. D.; Du Plessis, J.; Friend, J. R.; Yeo, L. Y. Toward complete miniaturisation of flow injection analysis systems: Microfluidic enhancement of chemiluminescent detection. *Anal. Chem.* **2014**, *86*, 10812−10819.
(24) Dovesi, R.; Orlando, R.; Erba, A.; Zicovich-Wilson, C.; Civalleri, B.; Casassa, S.; Maschio, L.; Ferrabone, M.; De La Pierre, M.; D'Arco, P. CRYSTAL14: A program for the *ab initio* investigation of crystalline solids. *Int. J. Quantum Chem.* **2014**, *114*, 1287−1317.
(25) Dovesi, R.; Saunders, V.; Roetti, C.; Orlando, R.; Zicovich-Wilson, C.; Pascale, F.; Civalleri, B.; Doll, K.; Harrison, N.; Bush, I.; D'Arco, P.; Llunell, M.; Causà, M.; Noël, Y. *CRYSTAL14 User's Manual*; University of Torino: Torino, 2014.
(26) Becke, A. D. Density-functional thermochemistry. III. The role of exact exchange. *J. Chem. Phys.* **1993**, *98*, 5648−5652.
(27) Grimme, S. Semiempirical GGA-type density functional constructed with a long-range dispersion correction. *J. Comput. Chem.* **2006**, *27*, 1787−1799.
(28) Civalleri, B.; Zicovich-Wilson, C. M.; Valenzano, L.; Ugliengo, P. B3LYP augmented with an empirical dispersion term (B3LYP-D*) as applied to molecular crystals. *CrystEngComm* **2008**, *10*, 405−410.
(29) Cora, F.; Patel, A.; Harrison, N. M.; Roetti, C.; Richard, A.; Catlow, C. An *ab initio* Hartree-Fock study of α-MoO_3. *J. Mater. Chem.* **1997**, *7*, 959−967.
(30) Berean, K. J.; Ou, J. Z.; Daeneke, T.; Carey, B. J.; Nguyen, E. P.; Wang, Y.; Russo, S. P.; Kaner, R. B.; Kalantar-Zadeh, K. 2D MoS_2 PDMS nanocomposites for NO_2 separation. *Small* **2015**, *11*, 5035−5040.
(31) Ou, J. Z.; Ge, W.; Carey, B.; Daeneke, T.; Rotbart, A.; Shan, W.; Wang, Y.; Fu, Z.; Chrimes, A. F.; Wlodarski, W.; Russo, S. P.; Li, Y. X.; Kalantar-Zadeh, K. Physisorption-based charge transfer in two-dimensional SnS_2 for selective and reversible NO_2 gas sensing. *ACS Nano* **2015**, *9*, 10313−10323.
(32) Jiao, Z. J.; Huang, X. Y.; Nguyen, N. T. Scattering and attenuation of surface acoustic waves in droplet actuation. *J. Phys. A: Math. Theor.* **2008**, *41*, 355502.
(33) Li, H.; Friend, J. R.; Yeo, L. Y. Surface acoustic wave concentration of particle and bioparticle suspensions. *Biomed. Microdevices* **2007**, *9*, 647−656.
(34) Rezk, A. R.; Ramesan, S.; Yeo, L. Y. Plug-and-actuate on demand: multimodal individual addressability of microarray plates using modular hybrid acoustic wave technology. *Lab Chip* **2018**, *18*, 406−411.
(35) Kang, J.; Seo, J.-W. T.; Alducin, D.; Ponce, A.; Yacaman, M. J.; Hersam, M. C. Thickness sorting of two-dimensional transition metal dichalcogenides *via* copolymer-assisted density gradient ultracentrifugation. *Nat. Commun.* **2014**, *5*, 5478.
(36) Bang, G. S.; Nam, K. W.; Kim, J. Y.; Shin, J.; Choi, J. W.; Choi, S.-Y. Effective liquid-phase exfoliation and sodium ion battery application of MoS_2 nanosheets. *ACS Appl. Mater. Interfaces* **2014**, *6*, 7084−7089.
(37) Lee, C.; Yan, H.; Brus, L. E.; Heinz, T. F.; Hone, J.; Ryu, S. Anomalous lattice vibrations of single- and few-layer MoS_2. *ACS Nano* **2010**, *4*, 2695−2700.
(38) Coleman, J. N.; Lotya, M.; O'Neill, A.; Bergin, S. D.; King, P. J.; Khan, U.; Young, K.; Gaucher, A.; De, S.; Smith, R. J.; Shvets, I. V.; Arora, S. K.; Stanton, G.; Kim, H.-Y.; Lee, K.; Kim, G. T.; Duesberg, G. S.; Hallam, T.; Boland, J. J.; Wang, J. J.; Donegan, J. F.; Grunlan, J. C.; Moriarty, G.; Shmeliov, A.; Nicholls, R. J.; Perkins, J. M.; Grieveson, E. M.; Theuwissen, K.; McComb, D. W.; Nellist, P. D.; Nicolosi, V. Two-dimensional nanosheets produced by liquid exfoliation of layered materials. *Science* **2011**, *331*, 568−571.
(39) Wu, J.-Y.; Lin, M.-N.; Wang, L.-D.; Zhang, T. Photo-luminescence of MoS_2 prepared by effective grinding-assisted sonication exfoliation. *J. Nanomater.* **2014**, *2014*, 852735.
(40) Tang, Y.; Zhang, X.; Choi, P.; Manica, R.; Liu, Q.; Xu, Z. Single-molecule MoS_2−polymer interaction and efficient aqueous exfoliation of MoS_2 into single layer. *J. Phys. Chem. C* **2018**, *122*, 8262−8269.
(41) Eda, G.; Yamaguchi, H.; Voiry, D.; Fujita, T.; Chen, M.; Chhowalla, M. Photoluminescence from chemically exfoliated MoS_2. *Nano Lett.* **2011**, *11*, 5111−5116.
(42) Alsaif, M. M. Y. A.; Field, M. R.; Daeneke, T.; Chrimes, A. F.; Zhang, W.; Carey, B. J.; Berean, K. J.; Walia, S.; van Embden, J.; Zhang, B.; Latham, K.; Kalantar-Zadeh, K.; Ou, J. Z. Exfoliation solvent dependent plasmon resonances in two-dimensional sub-stoichiometric molybdenum oxide nanoflakes. *ACS Appl. Mater. Interfaces* **2016**, *8*, 3482−3493.
(43) Xu, F.; et al. Scalable shear-exfoliation of high-quality phosphorene nanoflakes with reliable electrochemical cycleability in nano batteries. *2D Mater.* **2016**, *3*, 025005.
(44) Varrla, E.; Paton, K. R.; Backes, C.; Harvey, A.; Smith, R. J.; McCauley, J.; Coleman, J. N. Turbulence-assisted shear exfoliation of graphene using household detergent and a kitchen blender. *Nanoscale* **2014**, *6*, 11810−11819.
(45) Smith, R. J.; King, P. J.; Lotya, M.; Wirtz, C.; Khan, U.; De, S.; O'Neill, A.; Duesberg, G. S.; Grunlan, J. C.; Moriarty, G.; Chen, J.; Wang, J.; Minett, A. I.; Nicolosi, V.; Coleman, J. N. Large-scale exfoliation of inorganic layered compounds in aqueous surfactant solutions. *Adv. Mater.* **2011**, *23*, 3944−3948.
(46) Finn, D. J.; Lotya, M.; Cunningham, G.; Smith, R. J.; McCloskey, D.; Donegan, J. F.; Coleman, J. N. Inkjet deposition of

DOI: 10.1021/acs.chemmater.8b01506
Chem. Mater. 2018, 30, 5593−5601

liquid-exfoliated graphene and MoS_2 nanosheets for printed device applications. *J. Mater. Chem. C* **2014**, *2*, 925−932.
(47) Blonsky, M. N.; Zhuang, H. L.; Singh, A. K.; Hennig, R. G. *Ab initio* prediction of piezoelectricity in two-dimensional materials. *ACS Nano* **2015**, *9*, 9885−9891.

DOI: 10.1021/acs.chemmater.8b01506
Chem. Mater. 2018, 30, 5593−5601